Optimization of a Natural Graphite/Iron Phosphate Lithium-ion Cell

Venkat Srinivasan[*, 1] and John Newman[¥]

Energy and Environmental Technologies Division,
Lawrence Berkeley National Laboratory
Berkeley, CA-94720

Submitted as a technical paper to
The Journal of the Electrochemical Society

Original Submission: December 4, 2003
Revised Submission: February 28, 2004

[*] Electrochemical Society Active Member
[1] Author to whom correspondence should be addressed. e-mail: vsrinivasan@lbl.gov
[¥] Electrochemical Society Fellow

Abstract

This paper uses a model for a natural graphite/lithium hexafluoro phosphate (ethylene carbonate:diethyl carbonate)/iron phosphate lithium-ion cell in order to study its performance and aid in optimization. The model is used to generate Ragone plots for various designs, where both the average power of the cell and the peak power, defined at 80% depth-of-discharge for a 30 s pulse, are evaluated. This allows us to assess the ability of this chemistry to achieve the U. S. Department of Energy goals. The model is then used to maximize the specific energy of the cell by optimizing the design for a fixed time of discharge. The cell was optimized for the porosity and thickness of the positive electrode, while holding the capacity ratio of the two electrodes, the thickness and porosity of the separator, the electrolyte concentration, and the porosity of the negative electrode constant. The effect of the capacity ratio was qualitatively examined. The optimization was performed for discharge times ranging from 10 hours to 2 min in order to map the maximum performance of this chemistry under a wide operating range. The study allows us to gauge the ability of this chemistry to be used in a particular application. The optimized designs derived in this paper are expected to be a starting point for battery manufacturers and to help decrease the time to commercialization.

Introduction

The use of an energy storage device in a particular application requires consideration of a number of factors, such as, cost, specific energy, power capability, cycle life, calendar life and safety. The relative importance of each of these factors changes with the application, thereby making some energy-storage devices more suitable than others. For example, while an electric-vehicle battery would need to have high energy in order to extend the range, a hybrid-electric-vehicle battery would need more power capability for acceleration and regenerative braking. In order to aid in the design and manufacture of batteries for both these applications, the U.S. Department of Energy (DOE) provides goals for each of these factors.[1] These goals serve as a yardstick to decide if a particular chemistry is suitable for a given application.

While cost and life are decided, for the most part, by the choice of materials, the energy and power capability of a battery are also dependent on the design of the cell. A battery that is known to be well suited for low-power applications can be adapted for high-power applications by, for example, slicing the plates thinner and/or increasing the porosity. An example of this is the lead-acid cell where batteries used for starting, lighting, and ignition (SLI) have thinner plates and larger porosity compared to batteries for recreational marine use.[2] While this concept is well known intuitively, deciding how thin or how porous the plates need to be in order to optimize the performance requires a lot of experimentation involving building cells of various designs. Mathematical models provide an ideal alternative to this time consuming task by providing guidelines for the design and thereby reducing the experiments necessary. The goal of this paper is to illustrate the optimization methodology and provide the design for a wide range of applications using a modeling approach for a natural graphite/iron phosphate lithium-ion cell with a liquid electrolyte.

Tiedemann and Newman first illustrated the approach of optimizing porous electrodes to maximize the capacity by considering an ohmically limited battery, wherein activation and concentration polarization were assumed to be negligible.[3] The capacity maximum was seen to be a compromise between having more active material, accomplished by using thicker electrodes with low porosity, and the ensuing ohmic limitations in the solution phase. While this paper set out the methodology for optimization, the mass and energy of the system was not considered, and so the additional mass penalty arising from increasing the thickness, or decreasing the porosity, was left unaccounted. The effect of the mass was taken into account by Newman,[4] who showed the optimization of the same system by maximizing the specific energy. Newman identified a new dimensionless parameter that governs the optimum thickness and porosity of the electrode, namely,

$$T = \frac{U\kappa_s t_d}{q_+ L_s^2} \qquad [1]$$

where U is the open-circuit potential, κ_s the conductivity in the separator, t_d the time of discharge, q_+ the capacity density of the active material itself, and L_s the separator thickness. For systems with a reaction zone, Newman calculated the optimum thickness and porosity as a function of T. The author notes that the time of discharge, t_d, is the most significant factor that affects the design of the battery.[4] Fixing this quantity allows us to estimate T for a battery chemistry, and permits estimation of the optimum porosity and thickness. A parallel study to Newman's was undertaken by Dunn and Newman[5] for an electrochemical capacitor, where a parameter analogous to T was identified, using a simplified model wherein the reaction distribution in the porous electrode was assumed to be uniform (*i.e.,* the voltage *vs.* time was assumed to be linear, and the initial transients were neglected). In this study, the authors

optimized not only for the thickness and porosity of the electrodes, but also for the cut-off voltage of the cell. Both constant-current and constant-power operation were considered.[5]

While these studies had the advantage of having analytic solutions, they had the disadvantage of neglecting some of the factors that may be important in real cells (*e.g.,* mass transport). These can be accounted for by using a complete model for the battery, as illustrated by Fuller *et al.*[6] and Doyle *et al*.,[7-8] where the methodology for performing an optimization procedure, using Ragone plots, was highlighted. This procedure was used to its fullest extent by Thomas *et al.*[9] to optimize for a compromise between the specific energy and the peak specific power for a lithium-polymer cell. Such a compromise was first illustrated by Trost *et al.*[10] for the grid design of a lead acid cell where the size and mass of the battery plates were optimized.

This paper expands on the studies detailed above by taking a complete model for a natural graphite/iron phosphate Li-ion cell and optimizing for the porosity and thickness of the positive electrode while holding the porosity of the negative and the ratio of the positive to negative electrode capacity constant. We perform this study with the purpose of maximizing the specific energy for discharge times ranging from 10 hours to 2 min, to parallel the study performed by Newman.[4] This allows us to plot the maximum performance of this battery chemistry under a wide range of operating conditions spanning both the EV and the HEV needs. The methodology used in this study, when expanded to all other battery chemistries, should result in a map which can be used by researchers to pick a battery that suits their specific application.

In order to develop a model that represents the true behavior for this chemistry we compare the model to constant-current experiments for half-cells, with a lithium counter- and reference electrodes. Once this comparison is made, we simulate the behavior of the full cell and

perform the optimization studies. While the previous paper (reference 12) detailed the model-experimental comparisons for the lithium iron phosphate ($LiFePO_4$) electrode, we perform the comparison for the natural graphite (NG) electrode in this paper.

Model Development

Figure 1 shows the schematic of the cell modeled in this study, consisting of a natural graphite negative, pasted on a copper current collector, and a lithium iron-phosphate positive electrode, pasted on a carbon-coated aluminum current collector, with a separator between them. The whole cell is filled with 1 M lithium hexafluorophosphate ($LiPF_6$) in 1:1 ethylene carbonate (EC): diethyl carbonate (DEC) electrolyte. Both electrodes are assumed to be porous and made up of spherical particles. The processes during discharge are illustrated in the figure. The model equations used in this paper are the same as those described previously,[11] and hence will not be detailed here. Briefly, these consist of a mass balance and a modified Ohm's law in the electrolyte phase, Ohm's law in the solid phase, the Butler-Volmer equation, and a charge balance relating the reaction current to the solution current. The Butler-Volmer equation requires the concentration of lithium in the solid lattice at the particle surface. In the $LiFePO_4$ electrode, this is calculated by assuming that the phase-change and reaction occurs *via* a shrinking core, as described in the preceding paper[12] and illustrated in Figure 1. In the NG electrode, the diffusion equation is solved analytically for the time-dependent flux at the surface using the Duhamel superposition integral, as described by Doyle *et al.*[13] The model includes a film resistance, previously introduced by Doyle *et al.*,[7] in order to estimate the ohmic drop in the solid electrolyte interface (SEI) layer covering the graphite particles. This is accounted for by modifying the overpotential term in the Butler-Volmer equation by adding a voltage drop which

is related to the reaction current. The resulting equations were solved using the Band subroutine.[14]

The various transport, kinetic and thermodynamic parameters that are needed for the positive electrode are taken from the preceding paper.[12] For the NG electrode, we take the kinetic and transport parameters from the literature[15] and fit the model to experimental half-cell data to extract the ohmic parameters and the thermodynamic potential, as detailed below.

Model-Experimental Comparisons for the Natural Graphite Electrode

The experimental data used for the comparison is performed on NG powders prepared by Superior Graphite Co. (SL20) and has 90 wt% active material and 10 wt% poly vinylidene fluoride (PVDF) binder and has been studied extensively by Shim and Striebel.[16] The experiments reported in Figure 2 were performed by these authors on electrodes similar to ones reported in reference 16. All the electrode specific information is listed in Table 1. The experiments were conducted in Swegelok cells with lithium metal reference- and counter-electrodes. The reference electrode was placed between two pieces of separator. The electrode area was *ca.* 1 cm^2, and the mass was *ca.* 5.3 mg with 90 wt% active material and 10% binder. The capacity of the electrode was measured to be *ca.* 1.8 mAh/cm^2 based on a slow discharge.

The exchange current density used in previous models differ by more than an order of magnitude.[7, 15, 19] The value used here was chosen such that it was large enough to have little impact on the results. The SEI resistance has been estimated by both Doyle *et al.*[7] and Doyle and Fuentes[15] using fits of the model to experimental data. This quantity is possibly dependent on the thickness and the conductivity of the SEI layer and hence is used as a fitting parameter in this

study. Doyle and Fuentes[15] also use a current-collector resistance, which is extracted based on a model-experimental fits. Such a resistance was previously used by Arora *et al.* to fit a mathematical model of a Li-ion gel cell to experimental data.[17] A recent paper[18] examined the contact-resistance in NG electrode similar to the ones used in this study, and reported values that were considerably smaller than values reported by Doyle and Fuentes. Therefore, no contact-resistance was included in this paper. In a recent paper, Verbrugge and Koch[19] explore the intercalation of lithium into graphite using a combined model-experimental approach. The authors use a concentration-dependent diffusion coefficient, based on the data reported by Takami *et al.*,[20] with values changing by two orders of magnitude depending of the fractional occupancy. The resulting model was seen to be excellent in predicting the experimental discharge curves.[19] On the other hand, Doyle and Fuentes use a constant diffusion coefficient and were also able to predict the experimental data. While the change in diffusion coefficient can be expected to have an impact on the performance, incorporating it into a model results in complexities whereby a pseudo 2-D approach,[21] similar to the one used for the $LiFePO_4$ electrode, would need to be employed. Therefore, we decided to use a constant value for this quantity, which was taken to be the smallest value reported by Takami *et al.*[20] and used by Verbrugge and Koch.[19] Model-experimental comparisons (see Figure 2) suggest that the choice of diffusion coefficient provides adequate fits for the currents under which the experiments were conducted.

Various measurements of the thermodynamic potential for the graphite electrode have been performed in the literature. Thomas measured the equilibrium potential of this material as a function of state-of-charge (SOC) and fit an equation to the data.[22] A similar approach was taken by Verbrugge and Koch.[19] Both measurements show many similarities with the various plateaus

corresponding to the two-phase regions during intercalation and are also consistent with a slow-rate (*ca.* C/25, where the C-rate defined using the theoretical capacity of the electrode) discharge of the cell used in this study. Therefore, in this paper, we use an equation similar to that reported by Thomas,[22] but fit a low-rate (*ca.* C/25) discharge on these cells. The resulting equation is given by,

$$\begin{aligned} U(x) = {} & 0.124 + 1.5\exp(-70x) - 0.0351\tanh\left(\frac{x-0.286}{0.083}\right) - 0.0045\tanh\left(\frac{x-0.9}{0.119}\right) \\ & - 0.035\tanh\left(\frac{x-0.99}{0.05}\right) - 0.0147\tanh\left(\frac{x-0.5}{0.034}\right) - 0.102\tanh\left(\frac{x-0.194}{0.142}\right) \\ & - 0.022\tanh\left(\frac{x-0.98}{0.0164}\right) - 0.011\tanh\left(\frac{x-0.124}{0.0226}\right) + 0.0155\tanh\left(\frac{x-0.105}{0.029}\right) \end{aligned} \quad [2]$$

Where x represents the amount of lithium intercalated in the formula Li_xC_6. In summary, all the parameters except the resistance of the SEI are fixed. The experimental data are used to extract this quantity by fitting the voltage at different currents.

Figure 2 (a) shows the resulting model experimental fits using a SEI layer resistance of 0.023 Ω m^2. This is comparable in magnitude to the value used by Doyle and Fuentes (0.065 Ω m^2). The figure shows the ability of the model to describe the experimental data accurately, especially at the initial stages of the discharge. Deviations are seen in the final potential drop at higher currents, which could possibly be related to the use of the constant diffusion coefficient. However, when this electrode is used in a real cell with a $LiFePO_4$ positive electrode, the poor rate capability of the positive means that, under high-current operation, the negative electrode would not be reaching the end-of-discharge potential. This is illustrated in Figure 3 where discharge curves for the full-cell are simulated. However, it should be noted that under some

conditions (*e.g.,* very small $LiFePO_4$ particles, shown in Figure 4), the NG electrode reaches its end-of-discharge potential, thereby introducing errors in the predictions.

The mathematical model can now be used to estimate the various potential losses in the graphite electrode. This is performed for a current of 3.6 mA/cm^2, as illustrated in Figure 2 (b). The graph plots the equilibrium potential as discharge proceeds and the potential under a constant current for three conditions, namely (i) with the base case parameters; (ii) with no SEI resistance; and (iii) with a SEI resistance, but with a large solid-phase diffusion coefficient. The base-case curve is the same as the one shown in Figure 2 (a), and when compared to the equilibrium-potential curve, shows both a voltage drop and a lowered utilization. When the simulation is performed with no SEI resistance, the voltage drops in the electrode become negligible, as seen from the little difference between the electrode potential curve and the equilibrium potential. When the diffusion resistance is removed from the electrode, little change is seen in the voltage, but the electrode is now completely utilized, as seen from the fact that the curve reaches the equilibrium-potential curve at the end-of-discharge. This suggests that the main cause for the potential limitations in the graphite electrode is due to the potential drop through the SEI. While transport limitations start to play a part at the end-of-discharge, the contribution of this effect is limited, as seen from the small drop in utilization with increasing current.

Little can be done to improve the performance of the electrode shown in Figures 2(a) and (b). Transport limitations could be made less important by decreasing the particle size, but considering the relatively small losses seen in Figure 2(a), the improvement will not be substantial. In addition, comparisons of the NG electrode with the $LiFePO_4$ electrodes of similar design show that the utilization of the $LiFePO_4$ electrode is half that of the NG electrode,

suggesting that changes to the $LiFePO_4$ electrode are more critical. Reducing the voltage drops in Figure 2(a) necessitate decreasing the impact of the SEI. The SEI formation is an unavoidable side reaction, and its existence is thought to prevent further solvent decomposition. Decreasing the particle size may help in decreasing the reaction current (via the increased surface area for reaction) and thereby decrease the voltage drops through the SEI, but higher surface areas would lead to more SEI formation, which leads to a loss of lithium when used in a full cell, as described below. As the model does not include this side reaction, we do not attempt any changes to the particle size of the negative electrode. Finally, it is possible that additives can be used so that a stable SEI with little resistance is formed on the surface, thereby improving the performance of the electrode.

Simulation of the Natural Graphite/Iron Phosphate Cell

Having developed a model for both the NG and the $LiFePO_4$ electrodes, we now combine the two to simulate cell behavior. As each of the half-cell models have been compared to experimental data, we assume that the resulting cell model would adequately describe the performance of the full cell. The cell chosen is similar to that used by Shim and Striebel.[23] While the anode used is the same as the one detailed above, the cathode is considered to have 82 wt% active material, 4% carbon, 4% graphite, and 10% PVDF binder with an electrode capacity of 1.4 mAh/cm^2. Before simulations of discharge behavior are performed, an estimate of the initial state of the two electrodes needs to be made. This depends on the initial irreversible capacity loss and any other side reactions that may be occurring in the cell, and is, therefore, difficult to estimate. When the cell is first constructed, the lithium is in the $LiFePO_4$ electrode, with the graphite completely devoid of lithium. On the first charge, lithium deintercalates from

the positive and, while a fraction intercalates at the negative, the rest forms the SEI on the surface, and represents a loss of cycleable lithium. Estimates based on the first charge/discharge on these cells show that 18.6% of the total theoretical capacity of the negative electrode is lost to this side reaction. We therefore use this value in all our simulations. This allows us to calculate the loss of cycleable lithium. In addition, the final state of the battery at the end of the charge depends on the ratio of the positive and the negative electrodes.[8] For example, if the positive and negative electrodes were taken to have the same capacity, then at the end of the charge, all the lithium would be ejected from the positive, while at the negative, the lithium content would be 18.6% less than the maximum capacity. If, on the other hand, this ratio is changed, then the final x in Li_xC_6 would be different. We therefore calculate x based on the initial capacity ratio of the two electrodes and accounting for the capacity loss to the SEI.[24] This is the start of all the simulations in this paper. It should be noted that the 18.6% capacity fade may well be dependent on how much the negative electrode is charged in the first cycle (*i.e.,* a greater change in the voltage of the negative electrode may result in more SEI formation), which in turn may depend on the capacity ratio. However, this issue is ignored in this study. In all the simulations shown in this paper we do not change the surface-area-per-volume of the negative electrode, and hence the percent irreversible capacity (based on the total theoretical capacity of that electrode) is kept the same irrespective of the thickness of the electrode.

In general, lithium-ions cells are made with a larger anode capacity compared to that of the cathode in order to avoid any lithium deposition that can occur during high-current or pulse charging (or regenerative breaking when operating in an electric or hybrid vehicle). How much excess anode is used will decide how safe the battery will be from this deposition reaction. Arora *et al.* use a mathematical model to provide insight into the deposition process by

simulating the behavior under various charging regimes. However, having too large an excess would mean more capacity for SEI formation, as described above. We first take a cell, similar to the one used previously,[23] that has 29% excess anode capacity (defined as the difference in capacity of the anode and cathode, divided by the capacity of the cathode) and study its performance.

Figure 3 (a) plots the potential of the cell using the base-case parameters listed in Table 1 for a range of current densities, while Figure 3 (b) plots the corresponding electrode potentials. The electrode potentials denote the potential of the matrix at the current collector with respect to the potential of the solution at the mid-point of the separator, and hence, includes the resistance of the solution also. Note the significant decrease in the potential with increase in current and the large drop in the utilization in the figures. Figure 3 (b), which separates the losses in each of the electrodes, shows that a major portion of the potential losses are due to the positive electrode, arising from the significant ohmic limitations in the system. Figure 3 (b) also shows the change in the electrode limiting the end-of-discharge. At low currents, the iron-phosphate electrode is not limiting and therefore, the end-of-discharge occurs when all the lithium is extracted from the negative electrode. However, as the current increases, diffusion limitations in the positive electrode start to dominate this feature, and more and more lithium is left in the NG electrode at the end-of-discharge. Finally, at very large currents, the potential of the cell reaches the cut-off potential due to ohmic limitations much before diffusion limitations start to become important. Figure 3 shows that at larger currents the NG electrode does not discharge to points where there is little lithium left in the lattice. As noted in Figure 2, the model provides an excellent prediction of the cell voltage under these conditions, providing us with some confidence that the

neglect of the concentration-dependent diffusion coefficient in the negative electrode would have little impact on the results of this study.

Figure 3 suggests that changes to the design of the iron-phosphate electrode (increasing the conductivity, decreasing the particle size) would have a significant impact on performance. We study these design changes using Ragone plots, where the mass of the cell is taken to be that due to the electrodes (active material, carbon, binder), electrolyte, separator, and half the thickness of the two current collectors (as in a real cell both sides will be coated with active material). We do not include any mass arising from device packing or other related electronics.

Figure 4 plots the specific energy *vs.* the average specific power (Ragone plot) for the NG/$LiFePO_4$ cell for various designs (lines) and the specific energy for a 3 hour discharge and the peak specific power calculated at 80% depth-of-discharge (DOD) for a 30 s pulse (triangles). The figure also shows the DOE technology-assessment goals corresponding to the minimum goal for long-term commercialization (square). The Ragone plot is simulated for four cases (i) the base case listed in Table 1 [same as Figure 3(a)]; (ii) for the same parameters, but with a much larger matrix-phase conductivity in the iron-phosphate electrode; (iii) the cell in case (ii), but with the particle size of the iron-phosphate electrode decreased to 26 nm, and (iii) the cell in case (ii), but with the particle size of the iron-phosphate electrode decreased to 13 nm. This plot is analogous to Figure 8 in the previous paper,[12] but for a full-cell and on a mass basis. The improvement in performance with each of these modifications is clear, with the largest impact coming from the improvement in the conductivity of the positive electrode. While the decrease in the particle size from the base case of 52 nm to 26 nm results in an improvement in performance, a further decrease to 13 nm does not show an appreciable change. In the preceding paper,[12] decreasing the particle size to 13 nm was seen to show some improvement, although the

improvement was not substantial. However, when using this electrode in a full-cell, the transport limitations shift from the $LiFePO_4$ to the NG electrode as the particle size of the $LiFePO_4$ electrode is made smaller. Therefore, any change in particle size of the $LiFePO_4$ electrode does not have any impact on the performance. Clearly, one could also decrease the particle size of the NG electrode in order to improve the performance. This aspect is not explored in this study, considering the difficulties associated with calculating the amount of lithium lost to SEI formation with change in the surface area (resulting from the change in the particle size), as described previously. Figure 4 asserts that 26 nm particles for the iron-phosphate electrode would be sufficient to minimize transport limitations and improve performance. However, clearly, an increase in the matrix phase conductivity, for example, by doping,[25] or adding more carbon, is a critical step to make this electrode more competitive. Note that, in order to simulate cases (ii) to (iv), it is assumed that the matrix conductivity is made large without any mass penalty. This can be considered to be a doped $LiFePO_4$ electrode. Such an electrode was recently reported by Chung *et al.*[25] where an 8 order of magnitude increase in the conductivity was reported.

Figure 4 also shows the simulations corresponding to the goal defined by the DOE. This goal is defined as the specific energy for a 3 h discharge (taken from the point where the 3 h time-line intersects the Ragone plot for that cell design) plotted against the peak specific power. The peak specific power is estimated by discharging the cell until it reaches 80% DOD (2.4 h), and then finding the current under which the cell reaches the cut-off potential (2.5 V) in exactly 30 s. This was performed using a trial-and-error procedure until the required current is identified. The resulting specific energy and peak specific power is, therefore, a single point in the Ragone plot (represented by the triangles). For comparison, the DOE goals are also shown.

The increase in the peak specific power with each of the improvements in the cell design mirrors the increase in the average specific power. No change is seen in the peak power between the cells with 26 nm $FePO_4$ particles and 13 nm particles, and thus the peak power points for both cells coincide. In summary, Figure 4 shows that while the NG/$LiFePO_4$ cell shows potential in achieving the DOE power goals, the energy of the cell is significantly lower than that needed for long-term commercialization.

One strategy to improve the specific energy is to change the anode-to-cathode capacity ratio in order to maximize the amount of cycleable lithium in the cell.[8] As discussed above, a decrease in the anode mass (corresponding to a decrease in the capacity) would result in less SEI formation, and therefore result in less loss of lithium during the first cycle, providing more capacity during cycling of the cell. In addition, this decrease in the anode mass would decrease the total mass of the cell, thereby providing an increase in the specific energy. Competing with this is the danger of lithium deposition in cells that have little excess anode capacity. Therefore, one can expect an optimum based on these two competing effects. As the model developed in this paper does not include either the Li deposition reaction or the SEI formation reaction, this optimum is beyond the scope of this study. We however simulate various capacity ratio's to examine its impact on performance.

A second strategy is based on the fact that an analysis of the mass distribution in the cell shows that the current collectors occupy as much as 40% of the cell mass. Therefore, an increase in the mass of the active material so that the current collector occupies a smaller fraction of the cell mass, would result in an increase in the specific energy. This can be achieved by increasing the thickness and/or decreasing the porosity. However, an electrode that is too thick, or with little porosity, can be expected to have liquid-phase limitations, thereby limiting the performance

of the cell. Therefore, we expect an optimum for the thickness and porosity based on these competing effects. In order to identify the design that maximizes the specific energy, we use an optimization procedure, as described below.

Optimization of the Cell Design

Optimization procedure for a 3 h discharge:

The optimization in this paper is performed by varying the porosity and thickness of the positive electrode, while holding the porosity of the negative, the capacity ratio of the anode-to-cathode, the separator thickness and porosity, the salt concentration, and the particle size of the two electrodes constant. For the $LiFePO_4$ electrode, we use the 52 nm particles and a cell with no contact resistance and with a large matrix phase conductivity for this optimization. The goal of the optimization is to maximize the specific energy for a fixed time of discharge. A possible optimization of the anode involves changing the porosity and thickness while holding the capacity a constant, such that the anode-to-cathode capacity ratio is fixed. This was not performed in this study in order to minimize the number of variables that are optimized. As discussed later, we believe that this would have little impact on the trends reported in this paper. There is no optimum for the separator thickness; the smaller the thickness, the better the performance. The choice is limited by the ability of the separator to prevent a short. A value of 25 μm was used in this study. While the particle size of both electrodes has an impact on the performance (as shown in Figure 4), the material synthesis procedure may not allow for control of this quantity; hence the values used previous are left unchanged. Finally, we simulate the iron-phosphate electrode with a large matrix-phase conductivity and no contact resistance as recent developments suggest that both these improvement are possible with the use of carbon-

coated current collectors to remove the contact resistance, and the use of extra conductive carbon in the matrix, or *via* the use of doped[25] iron-phosphate electrodes.[26]

The first step in the optimization is to fix the excess anode capacity. We start with a cell with the base capacity ratio of 29%, but we also illustrate two other ratio's. Once this quantity is fixed, we decide on the discharge time. Newman points out that this is the most important factor for the design of the battery.[4] The time of discharge is decided by the application. For example, for EV applications, a 3 hour discharge is applicable, while for a photovoltaic application, a 6 to 10 hour discharge is generally needed. Any cell design would necessarily have to satisfy this time of discharge goal. Once this is defined, we pick a porosity and thickness of the positive electrode, and find the current which would make this battery reach its cut-off potential (taken as 2.5 V in this study) at exactly the time of discharge. In other words, if we pick a current such that the battery reaches the cut-off in less than the discharge time, then this is deemed a design that is not appropriate. On the other hand, if the current were such that the battery discharges for more than the specified discharge time, then there would be capacity wasted at the end of discharge, and hence would lead to a decrease in the energy. Hence a larger current can be used for the discharge. The optimum current was identified using trial-and-error. After the identification of the optimum current, the specific energy is calculated for this design. Subsequently a new design is picked, and the procedure repeated to estimate the corresponding specific energy. This is repeated until we identify the maximum specific energy at that time of discharge. In all the simulations, the ratios of the active material to carbon and active material to binder were kept constant, and the mass was calculated.

The optimum in the thickness and the impact of the capacity ratio of the two electrodes is illustrated in Figure 5, where the specific energy is plotted against the positive electrode

thickness for three values of the capacity ratio. In all these plots, the porosity of the cell is held fixed at the base-case values. Note that, as the capacity ratio is fixed in each of these lines, a change in the positive-electrode thickness would mean a corresponding change in the negative-electrode thickness. The symbol (♦) represents the value for the base-case cell taken from Figure 4. As the positive electrode thickness is increased, more capacity (and consequently, energy) is added into the cell, and the mass of the current collectors become a smaller fraction of the cell mass, thereby resulting in an increase in the specific energy. However, the competing effect of the increasing liquid-phase transport limitations start to become important at larger thickness, and an optimum is reached at *ca.* 500 μm. However, note that even at this optimum, the energy is lower than the DOE goal (shown by the horizontal dashed line).

When the anode-to-cathode capacity ratio is decreased to 10%, the nature of the curves remains the same, but with the specific energy higher at all thicknesses. As the anode is made smaller, two beneficial effects, namely, a decrease in the overall mass of the cell and the decrease in the loss of cycleable lithium due to SEI formation, increase the specific energy of the cell. This increase would continue to occur as the anode capacity is decreased further, and hence a series of curves at each ratio can be drawn. The smaller the ratio, the greater the chances of Li deposition during high–current or pulse charging. The maximum one can reach with this strategy is to make the capacity of the cathode such that it is equal to the sum of the capacity of the anode and the capacity lost to SEI formation.[8] This would represent a perfectly balanced cell and shows the maximum energy, as illustrated in Figure 5. This configuration would be extremely susceptible to Li deposition and would never be a practical cell, but it serves to identify the maximum possible specific energy of this cell. Note that this maximum is lower than the DOE long-term technology assessment goal (200 Wh/kg for a 3 hour discharge). We

choose the design with a 10% excess for further study as this provides an ideal compromise between minimizing Li deposition while achieving the DOE's minimum goal for long-term commercialization. Clearly, a model which includes both the SEI formation reaction and the Li deposition reaction would be extremely useful in predicting how much excess anode is needed in order to compromise between these two quantities.

Figure 5 was generated for a positive-electrode porosity of 0.27. When the cell with the 10% excess anode capacity is simulated with different porosities, both the optimum porosity and thickness are identified, as shown in Figure 6. This figure is similar to Figure 5 in that it plots the specific energy as a function of the positive-electrode thickness. Three values of positive electrode porosity are shown in the figure, with the base case (0.27) taken from Figure 5. In all these figures, the negative-electrode porosity is left unchanged. Note that as the ratio of the capacity of the anode to cathode is maintained at 10%, a change in the positive-electrode porosity for the same positive-electrode thickness would result in a different negative electrode thickness. As the porosity of the positive electrode is decreased, more active material is packed into the cell, and the current collectors occupy a smaller fraction of the cell mass, resulting in an increase in the specific energy. However, similar to increasing the electrode thickness, this leads to greater losses in the solution phase, and so an optimum is reached, as seen in the curve at a porosity of 0.12, where a smaller specific energy is seen compared to a porosity of 0.19. However, the effect of the porosity is not as pronounced as that for the thickness. Note that, as the porosity is decreased, the optimum thickness decreases. This occurs because of the need to minimize transport limitations in the cell, which necessitates a smaller thickness for a smaller porosity. Figure 6 can be used to identify the optimum porosity and thickness of the positive electrode to maximize the specific energy for a 3 h discharge. This occurs at a positive-electrode

porosity of 0.19, a positive-electrode thickness of 410 μm and a negative-electrode thickness of *ca.* 260 μm. A plot similar to Figure 6 can be made for any time of discharge in order to find the optimum design for other applications.

The performance of the optimized cell can now be compared to the original cell, as shown the Ragone plots of the two cells in Figure 7. The plot also shows the simulated peak power for the cells. Note that while the optimized cell shows significant increase in the specific energy, this comes at a loss of specific power. This loss is seen both in the average-power and the peak-power values. While the cell optimized for a 3 h discharge shows an invariant energy during low-power operation, discharging the cell faster than 3 hours results in a significant decrease in the energy of the cell. Clearly the cell optimized for specific energy is not suited for high-power operation, necessitating a compromise between the energy and power capability.

Trost *et al.*[10] show one way of optimizing for a compromise between the specific energy and the maximum specific power at 50% DOD. The authors show this by changing the mass of the grid for a specified plate size (defined as a square root of the area), length of the bus, and length of the post for a lead-acid cell. The authors calculate these quantities for a 4 hour discharge. First the authors plot the specific energy *vs.* the maximum power for varying grid mass. This gives them a loop in the power and energy which starts at zero for a grid of zero mass (*i.e.,* no current can be collected when there is no grid) and ends at zero for a grid of infinite thickness (*i.e.,* the mass of the grid is infinitely large such that both specific energy and power are zero). From this plot, Trost *et al.* identify the maximum in both the specific energy and the power and take the compromise as the design that gives a ratio equal to the ratio of these two quantities. The authors then repeat this procedure for a different plate size and identify the maximum compromise design for the cell. An alternate formulation was suggested by Thomas

et al.,[9] where the thickness and porosity of a V_6O_{13} electrode in a Li-polymer cell were optimized for a compromise between the specific energy and the peak specific power at 80% DOD for a 30 s pulse. Here the authors calculate the product of these two quantities for various cell designs, and identify the design that gives them the maximum. This is defined as the compromise between energy and power.

Both these studies achieve a compromise for a particular application and provide the best possible design for that application. However, the optimization does not provide any information on the ability of this cell to be used in another application. For example, while the peak discharge specific power is defined at 80% DOD for a EV system, for the same battery to be optimized for regenerative braking, the optimization would need to be performed at 20% DOD. Optimizing for one of these quantities does not allow us to gauge the ability of the chemistry to satisfy the other. Therefore, it was decided that the optimization would be performed without any peak pulse operations, but for a range of discharge times, such that all applications ranging from photovoltaic to HEVs can be covered. This can be thought of as a parallel to the approach taken by Newman (see Figure 10 in reference 4). Therefore, the procedure illustrated above for maximizing the specific energy for a 3 h discharge was repeated for other times of discharge, and the design for each discharge time identified.

Optimization for varying discharge times:

Figure 8 shows the results of such an optimization procedure, where a Ragone plot is shown with the envelope curve (solid line) that maps the maximum performance of this cell over discharge times ranging from 10 h to 2 min. This plot has a different design at each point (see Figures 9 and 10 for the design). The plot also shows the results of taking one of these cells and using it under other applications. For example, a cell optimized for a 3 h discharge application

performs adequately for longer discharge times, but has poor performance at shorter discharge times. As longer discharge times have thicker electrodes with less porosity, these cells are susceptible to large liquid-phase limitations, and hence operation under higher currents result in large losses. In order to use this chemistry for higher-power applications, the cell design will need to be changed. Two examples of this are given in Figure 8. For example, if a 30 min discharge time were desired, a cell optimized for that discharge time would be built. However, as illustrated in Figure 8, this cell, when used under other conditions, shows losses in energy at longer discharge times and losses in power at shorter discharge times. While the former occurs because the electrodes are not large enough to minimize the impact of the current collectors, the latter occurs because the electrode are too large for higher-power operation where losses in the solution phase become important. In summary, Figure 8 asserts that while a battery designed for one application may be inadequate for a different application, a change in the design could make it satisfy the needs of this application. The figure also gives an indication of how much the losses are when not operating at the design for which it is optimized. Figure 8 also shows the DOE goal for comparison. While a true conclusion as to ability of this chemistry to attain the DOE goal can be made only by performing the optimization for the compromise, as mentioned previously, the fact that the knee of the Ragone plot is much lower than the DOE goal, suggests that achieving the goal may be difficult.

Figure 9 (a) and (b) show the design resulting from the optimization studies. Figure 9 (a) plots the thickness of the positive and negative electrodes while Figure 9 (b) shows the porosity of the positive electrode for the various discharge times (corresponding to the dotted lines in Figure 8). Note that the negative electrode porosity was not changed in the simulations, and that the negative-electrode thickness is a consequence of the assumption that the anode-to-cathode

capacity ratio is held constant. The figure follows the expected trend that high-power operation requires thinner electrodes and greater porosity compared to low-power operation. The figure shows that the design changes significantly with the time of discharge, with values ranging from a thickness of 550 μm and a porosity of 0.15 for 10 hour operation to 135 μm and 0.34 for a 2 min discharge.

The optimum current density corresponding to the envelope plot in Figure 8 is shown in Figure 10. For a particular discharge time, a cell built with the design shown in Figure 9, when discharged at the optimum current, shown in Figure 10, would result in the battery potential reaching 2.5 V at exactly the discharge time. As noted by Thomas *et al.*, the current required for a given application is decided by the load.[9] Therefore, one could use the optimum in Figure 10 to estimate the optimum area of the electrode to sustain this load. Figure 9 and 10 provide a starting point for an electrode-development program and provides guidelines for cell design for a wide variety of applications. The values that are used in these figures are listed in Table 2 for convenience.

Various solutions can be devised in order to improve the performance of the system and help it achieve the DOE goals. In this study we have maintained the anode porosity constant. One could adjust the porosity and thickness of the anode while keeping its capacity constant, such that the anode-to-cathode capacity ratio is maintained. During discharge, the concentration of lithium in the solution phase increases in the anode, leading to a decrease in the conductivity as it crosses the conductivity maximum. Thicker anodes may therefore experience liquid-phase limitations, which could be ameliorated by optimizing also over the porosity of the negative electrode. However, thicker anodes are needed only when the discharge time is large (as seen for the positive electrode in Figure 9), and under these conditions the concentration would not rise in

the anode significantly since there would be adequate time for the concentration to equilibrate across the cell. During high-power operation, the thickness of the electrode is small, and the porosity used in this study (0.33) is large enough that limitations should be minimal. Therefore, we believe that even if this quantity were optimized for, the improvements would not be significant. One could decrease the anode mass in the cell even further in order to increase the amount of cycleable lithium. As seen in Figure 5, this can have a significant impact on the specific energy. While this would increase the probability of lithium deposition, it is not clear as to how much excess is actually needed. Natural graphite is thought to have more first cycle irreversible capacity loss compared to MCMB carbons, and hence the final x in Li_xC_6 would be lower in NG for the same amount of excess anode capacity. It is possible that a more detailed understanding of the first-cycle loss and the lithium deposition reaction would help to see whether this ratio can be decreased further. As shown in Figure 4, decreasing the particle size helps in increasing the power capability of the cell. It is possible that optimizing a cell with a smaller particle size may indeed provide greater power capability for these cells. Another strategy is to increase the concentration of the salt. Considering that transport limitations are very important in thick cells, higher concentrations may help in offsetting these limitations. However, this will enhance the risk of precipitating the salt, especially in the anode.[8] Finally, the size of the current collectors used in this study is probably larger than those in real cells. Decreasing the size of the current collectors will help in decreasing the mass of the cell and thereby increase the specific energy. However, real cells have additional mass arising from device packing and related electronics, which are not included in this model. Incorporation of this added mass may offset the higher current-collector weight used here.

The optimum values that are predicted in Figure 9 depends on the added mass in the cell. Newman provides an estimate for the change in the optimum design with an increase in the residual mass of the cell.[4] The author shows that as the residual mass increases, both the optimum thickness and porosity increase for all times of discharge. A residual mass that is 10 times the mass of the separator results in an approximate doubling of the thickness and a 40% increase in the porosity over a range of discharge times. A better estimate of the actual residual masses in a cell, including the size of the current collectors, would help in making these optimizations more accurate. However, one could use the methodology illustrated in this paper for a variety of Li-ion chemistries, all with the same residual mass as that used in this paper, and get a performance map of the various chemistries. Such a plot would be extremely helpful in assessing the usefulness of a particular chemistry when used for a specific application. Finally, manufacturing difficulties could impose constraints on the maximum thickness and minimum porosities that an electrode can be fabricated at. While this would decrease the performance compared to those shown here, the model provides an ideal route for exploring the penalty of such constraints.

Conclusions

The ability of a battery chemistry to be used for a particular application requires proper cell design. This paper uses a mathematical model as a tool to optimize the design for a natural graphite/iron phosphate lithium-ion cell with a liquid electrolyte. Simulation of Ragone plots where both the average power and the peak power of the cell, calculated at 80% DOD for a 30 s pulse, showed that the cell performance was considerably lower than the DOE goals. Elimination of the ohmic drops and a reduction in particle size of the positive electrode were

seen to be helpful in increasing the power capability of the cell. Particle sizes less than 26 nm for the positive electrode showed no improvement in performance because of limitations shifting to the negative electrode.

In order to improve the specific energy of the cell, an optimization procedure was initiated. The cell was optimized for the porosity and thickness of the positive electrode, while holding the capacity ratio of the two electrodes, the thickness and porosity of the separator, the electrolyte concentration, and the porosity of the negative electrode constant. The time of discharged was varied from 10 h to 2 min in order to map the maximum performance of this material under all applications. The effect of changing the capacity ratio of the electrodes was qualitatively studied.

The optimization studies show that while the DOE energy goals for a 3 hour discharge can be achieved, achieving the power goals may be more challenging for the cell chosen. Possible solutions to improve performance include decreasing the particle size of the electrodes, removing excess anode capacity, increasing the salt concentration, and removing the residual mass of the cell. Slower discharge times allowed for thicker electrodes with less porosity in order to minimize the impact of the current collectors. Faster discharges require thinner cells with more porosity in order to minimize liquid-phase limitations. While electrode thicknesses in the order of 550 μm and a porosity of 0.15 were obtained for 10 hour operation, for a 2 min discharge, a thickness of 135 μm and a porosity of 0.34 were estimated. Estimating the maximized specific energy for a variety of Li-ion chemistries for a range of discharge times would provide a means for gauging the applicability of a particular chemistry for a given application.

Acknowledgements

Financial support from the Assistant Secretary for Energy Efficiency and Renewable Energy, Office of FreedomCAR and Vehicle Technologies of the U.S. Department of Energy under Contract No. DE-AC03-76SF00098 is gratefully acknowledged. We acknowledge Kathy Striebel and Joongpyo Shim (LBNL) for providing the experimental data used in Figure 2.

References

1. http://ott.doe.gov

2. D. Linden, *Handbook of Batteries,* 2nd edition, McGraw Hill, New York, p. 24.36 (1994).

3. W. Tiedemann and J. Newman, *J. Electrochem. Soc.*, **122**, 1482 (1975).

4. J. Newman, *J. Electrochem. Soc.*, **142**, 97 (1995).

5. D. Dunn and J. Newman, *J. Electrochem. Soc.*, **147**, 820 (2000).

6. T. F. Fuller, M. Doyle, and J. Newman, *J. Electrochem. Soc.*, **141**, 1 (1994).

7. M. Doyle, J. Newman, A. S. Gozdz, C. N. Schmutz, and J.-M. Tarascon, *J. Electrochem. Soc.*, **143**, 1890 (1996).

8. C. M. Doyle, *Design and Simulation of Lithium Rechargeable Batteries*, PhD. Dissertation, University of California, Berkeley (1995).

9. K. E. Thomas, S. E. Sloop, J. B. Kerr, and J. Newman, *J. Power Sources*, **89**, 132 (2000).

10. G. G. Trost, V. Edwards, and J. Newman, *Chemical Reaction and Reactor Engineering,* J. J. Carberry and A. Varma, Editors, Marcel Dekker, Inc., New York, p. 923-972 (1986).

11. K. E. Thomas, R. M. Darling, and J. Newman, in *Advances in Lithium-Ion Batteries*, W. van Schalkwijk and B. Scrosati, ed., New York: Kluwer Academic/Plenum Publishers, 345 (2002).

12. V. Srinivasan and J. Newman, *Discharge Model For The Lithium Iron-Phosphate-Electrode*, *J. Electrochem. Soc.*, Submitted (2003).

13. M. Doyle, T. F. Fuller, and J. Newman, *J. Electrochem. Soc.*, **140**, 1526 (1993).

14. J. Newman, *I&EC Fundamentals*, **7**, 514 (1968).

15. M. Doyle and Y. Fuentes, *J. Electrochem. Soc.*, **150**, A706 (2003).

16. J. Shim and K. A. Striebel, *J. Power Sources*, **119-121**, 934 (2003)

17. P. Arora, M. Doyle, A. S. Gozdz, R. E. White, and J. Newman, *J. Power Sources,* **88**, 219 (2000).

18. C.-W. Wang, K. A. Cook, and A. M. Sastry, *J. Electrochem. Soc.*, **150**, A385 (2003).

19. M. W. Verbrugge and B. J. Koch, *J. Electrochem. Soc.*, **150**, A374 (2003).

20. N. Takami, A. Satoh, M. Hara, and T. Ohsaki, *J. Electrochem. Soc.*, **142**, 371 (1995).

21. B. Paxton and J. Newman, *J. Electrochem. Soc.*, **143**, 1287 (1996).

22. K. E. Thomas, *Lithium-Ion Batteries: Thermal and Interfacial Phenomena,*, PhD. Dissertation, University of California, Berkeley (2002).

23. J. Shim and K. A. Striebel, *J. Power Sources*, **119-121**, 955 (2003).

24. P. Arora, M. Doyle, and R. E. White, *J. Electrochem. Soc.*, **146**, 3553 (1999).

25. S. –Y. Chung, J. T. Bloking, and Y. –M, Chiang, *Nature Mat.*, **2**, 123 (2002).

26. K. Striebel, J. Shim, V. Srinivasan, and J. Newman, Abstract 348, The Electrochemical Society Extended Abstracts, Orlando, Fl, Oct 12-16, 2003.

27 C. Capiglia, Y. Saito, H. Kageyama, P. Mustarelli, T. Iwamoto, T. Tabuchi, and H. Tukamoto, *J. Power Sources*, **81-82**, 859 (1999).

Table 1. Table of design-adjustable parameters, electrode specific parameters, and other constants used in the paper. The values correspond to the base-case simulations in the text.

Design-adjustable Parameters		
Parameter	**Natural Graphite**	**Iron Phosphate**
Electrode thickness (μm)[a]	50	75
Electrode porosity[b]	0.33	0.27
Weight percent of carbon additive[a]	-	4
Weight percent of graphite additive[a]	-	4
Weight percent of PVDF[a]	10	10
Average particle radius (R_{avg})[a]	11 μm	52 nm
Small particle radius[c]	-	$R_{avg}/1.2$
Large particle radius[c]	-	$R_{avg}\times1.8$
Current collector thickness (μm)[a]	25	30
Electrode Parameters		
Parameter	**Natural Graphite**	**Iron Phosphate**
Diffusion coefficient in solid (m^2/s)	9×10^{-14} [d]	8×10^{-18} [c]
Exchange current density at a reference concentration of 1M and x=0.1, y=0.5 (A/m^2)	500	3.14×10^{-6} [c]
Matrix phase conductivity (S/m)	100 [e]	5×10^{-3} [c]
Contact resistance ($\Omega\ m^2$)	0	0.0065 [c]

Electrolyte/separator Properties	
Parameter	**Value**
Salt Diffusion Coefficient (m^2/s)[f]	$D = 5.34 \times 10^{-10} \exp(-0.65c)$
Transference number of lithium[f]	0.4
Conductivity (S/m)[g]	$\kappa = 0.0911 + 1.9101c - 1.052c^2 + 0.1554c^3$
Separator thickness (μm) [h]	25
Separator porosity [h]	0.55
Initial salt concentration (M)[a]	1
Densities (g/cm^3)	
Parameter	**Value**
$LiFePO_4$	3.6
Graphite	2.27
Carbon black	1.75
Separator	0.9
Electrolyte	1.2
Copper	8.9
Aluminum	2.7

a Measured
b Estimated
c Model fits (see reference 12)
d Smallest reported value in reference 20
e Large enough to have no impact on the results (*i.e.,* $\sigma >> \kappa$)
f From reference 27 for LiPF6 in EC:EMC
g From reference 8
h see http://www.celgard.com/documents/Celgard_2500.pdf

Table 2. The optimized designs that provide the maximum specific energy at each discharge time obtained using this study. The table corresponds to Figures 9 and 10. Note that the negative electrode porosity was held constant at 0.33.

Discharge time (h)	Thickness-positive electrode (μm)	Porosity-positive electrode	Thickness-negative electrode(μm)	Optimum current density (A/m^2)
10	550	0.15	364.46	8.99
3	410	0.19	258.9	21.1
1	285	0.23	171.0	40.9
0.5	220	0.25	128.6	59.4
0.25	180	0.27	102.4	83
0.0833	150	0.31	80.7	123
0.0333	135	0.34	69.4	145

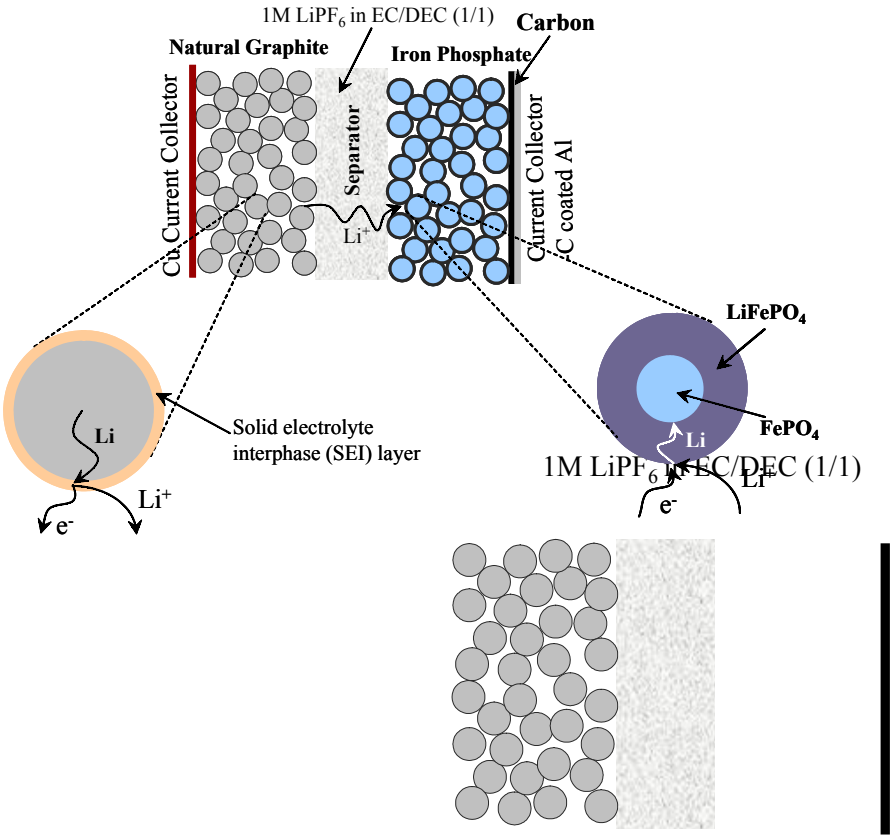

Figure 1. Schematic of the cell modeled in this study consisting of a natural graphite negative and an iron phosphate positive electrode with a separator between them. The whole cell is filled with 1 M $LiPF_6$ in EC/DEC (1:1). The processes on discharge are illustrated in the figure. Lithium transport *via* a diffusion mechanism and ohmic losses through the SEI are described for the negative electrode. The transport of lithium through the shell and the movement of the phase interface are described for the positive electrode.

(a)

(b)

Figure 2. Model-experimental comparisons of the graphite half-cell at various currents (a) and the corresponding potential drops in the electrode at a current of 3.6 mA/cm^2 (b). The SEI layer resistance is used as a fitting parameter in the figures, while the rest of the parameters are taken from the literature. Figure 3 (b) shows the decomposition of the electrode potential curve by plotting the equilibrium potential, the electrode potential with no SEI layer and the electrode potential with no diffusion resistance.

(a)

(b)

Figure 3. Simulated cell potential (a) and individual electrode potentials (b) at different current densities during discharge of a NG/$LiFePO_4$ cell. The curves were generated using the base-case parameters in Table 1. The electrode potentials were generated by plotting the potential of the matrix at the current collector minus the potential of the solution at the mid-point of the separator. Note the significant drops in the potential of the positive electrode.

Figure 4. Simulated Ragone plot of the NG/$LiFePO_4$ cell for various designs. The lines represent the average specific power of the cell (*i.e.,* specific energy divided by the discharge time) while the symbols represent the specific energy evaluated from a 3 h discharge and the peak specific power defined at 80% DOD for a 30 s pulse. The DOE technology-assessment minimum goal for long-term commercialization is also shown.

Figure 5. Illustration of the optimum in the positive electrode thickness for maximizing the specific energy for a constant porosity of 0.27 for the positive electrode. The plot also shows the effect of the anode to cathode capacity ratio. The DOE goal is shown for comparison. Each point is generated by finding the optimum current such that the cell discharges to 2.5 V in 3 h. Note that the negative electrode thickness is changed correspondingly. The symbol ♦ represents the value taken from Figure 4.

Figure 6. Illustration of the effect of porosity on the optimum thickness with the anode-to-cathode capacity ratio fixed at 10%. The curve at a porosity of 0.27 is same as that in Figure 5. Each point is generated by finding the optimum current such that the cell discharges to 2.5 in 3 h. Note that the negative electrode thickness is changed correspondingly. The optimum design occurs at ε_+=0.19 and L_+=410 μm.

Figure 7. Comparison of the performance of the cell using the base-case design from Table 1 and the optimized design from Figure 6 for a 3 h discharge. The plot shows a Ragone plot with both the average power and the peak power defined at 80% DOD for a 30 s pulse.

Figure 8. Ragone plot of the NG/$LiFePO_4$ cell with various optimized designs. The solid line is the envelope curve where every point is optimized for the corresponding discharge time. The design is shown in Figure 9, and the optimum current in Figure 10. The plot also shows the performance of three cells which are designed for one discharge time and used under other conditions. Compare with Figure 10 in reference 4.

(a)

(b)

Figure 9. Optimized thickness and porosity corresponding to the envelope plot in Figure 8. A cell fabricated with the design shown here would yield the maximum specific energy at that discharge time. The optimization was performed for the positive electrode thickness and porosity. The excess capacity ratio of the anode to cathode was held constant at 10% while the negative-electrode porosity was held constant at 0.33, and hence the negative-electrode thickness changes corresponding to the change in design of the positive electrode.

Figure 10. Optimized current density corresponding to the envelope curve in Figure 8. The current density can be used to decide the area required to satisfy a specified load requirement.